

Seismic Performance of Underground Reservoir Structures: Insight from Centrifuge Modeling on the Influence of Backfill Soil Type and Geometry

A. Hushmand, S.M.ASCE¹; S. Dashti, M.ASCE²; C. Davis, M.ASCE³; B. Hushmand⁴;
J. S. McCartney, M.ASCE⁵; J. Hu, M.ASCE⁶; and Y. Lee, M.ASCE⁷

Abstract: The seismic response of underground reservoir structures is a complex soil–structure interaction problem that depends on the properties of the earthquake motion, surrounding soil, and structure. More experimental and field data of the response of these structures under different boundary conditions are needed to validate analytical and numerical tools. This paper presents the results of four centrifuge experiments that investigate the seismic performance of reservoir structures, restrained from rotational movement at their roof and floor, buried in dry, medium-dense sand and compacted, partially saturated, silty sand. This study focuses on the influence of backfill soil properties, cover, and slope on accelerations, strains, lateral distortions, and lateral earth pressures experienced by the buried structure. The structure to far-field acceleration spectral ratios were observed to approach unity with added soil confinement, density, and stiffness. Both dynamic thrust and accelerations on the structure showed a peak near the effective fundamental frequency of the backfill soil. The addition of a shallow soil cover and stiffness slightly increased seismic earth pressures and moved their centroid upward, hence slightly amplifying seismic moments near the base. The added stiffness, density, and apparent cohesion of the compacted site-specific soil did not influence the magnitude of dynamic earth pressures significantly but often moved their centroid upward. A sloping backfill reduced the earth pressures and bending moments near the top of the wall because of the reduced soil mass. The trends in the experimental results indicate that new analytical procedures and design guidelines are needed to account for the backfill soil conditions and ground motions for which these underground structures must be designed. DOI: [10.1061/\(ASCE\)GT.1943-5606.0001544](https://doi.org/10.1061/(ASCE)GT.1943-5606.0001544). © 2016 American Society of Civil Engineers.

Author keywords: Underground reservoir structure; Soil–structure interaction; Centrifuge modeling; Seismic earth pressures.

Introduction

An experimental study was conducted on the seismic response of shallow-buried reservoir structures. This study was inspired by the design of prototype reinforced concrete buried reservoirs (e.g., the Headworks reservoir under construction) in Los Angeles to replace open-water reservoirs for the purpose of improving water quality and safety. These reservoir structures have 11- to 12-m-high walls that will be buried after construction. They are restrained against rotational movement at the top and bottom by a roof and floor, restricting their deformation, unlike yielding retaining walls.

However, they are also not completely rigid and deform according to their flexural stiffness. Hence, they are classified as stiff-unyielding structures (Hushmand et al. 2014, 2016). The reservoirs will be covered with a shallow layer of compacted silty sand with a 2:1 sloped embankment on either side. The structure's foundation can rock or slide laterally, as it rests on a prepared soil subgrade. Soil–structure interaction (SSI) for these buried structures is complex and depends on the properties of the earthquake motion, properties and geometry of the surrounding soil, foundation fixity, and the flexibility of structure relative to soil. There is an increasing need in engineering practice to obtain a better understanding of the seismic performance of these stiff-unyielding underground structures for a range of surrounding soil and loading conditions.

¹Graduate Student Researcher, Dept. of Civil, Environmental, and Architectural Engineering, Univ. of Colorado Boulder, Boulder, CO 80309.

²Assistant Professor, Dept. of Civil, Environmental, and Architectural Engineering, Univ. of Colorado Boulder, Boulder, CO 80309 (corresponding author). E-mail: shideh.dashti@colorado.edu

³Trunk Line Design Manager, Los Angeles Dept. of Water and Power, 111 North Hope St., Los Angeles, CA 90012.

⁴President and Principal Engineer, Hushmand Associates, Inc., 250 Goddard, Irvine, CA 92618.

⁵Associate Professor, Dept. of Structural Engineering, Univ. of California, San Diego, La Jolla, CA 92131.

⁶Civil Engineering Associate, Los Angeles Dept. of Water and Power, 111 North Hope St., Los Angeles, CA 90012.

⁷Civil Engineering Associate, Los Angeles Dept. of Water and Power, 111 North Hope St., Los Angeles, CA 90012.

Note. This manuscript was submitted on August 12, 2015; approved on March 22, 2016; published online on June 16, 2016. Discussion period open until November 16, 2016; separate discussions must be submitted for individual papers. This paper is part of the *Journal of Geotechnical and Geoenvironmental Engineering*, © ASCE, ISSN 1090-0241.

The available simplified methods used to estimate seismic lateral earth pressures on the walls of underground structures are limited in several ways, preventing their reliable application to the design of reservoir structures. For example, the kinematic constraints of the structures at their roof and base against rotation are quite different from the assumption of yielding or active conditions by Mononobe-Okabe (M-O) (Okabe 1926; Mononobe and Matsuo 1929) or Seed-Whitman (S-W) (Seed and Whitman 1970). Further, the walls of these structures are not completely rigid and deform depending on their stiffness, which is different from the rigid assumption behind the simplified Wood (1973) procedure. Also, none of the available simplified analytical methods consider the complexities introduced by soil cover, backfill slope, and apparent cohesion of the backfill soil.

A few important parameters used in the seismic design of buried reservoir structures include dynamic lateral earth pressures, bending moments, and the lateral distortions induced by earthquake

loading. A time history analysis of the soil–structure system is typically warranted to obtain these parameters for design. However, numerical simulations of these structures (e.g., Harounian et al. 2014; Zhai et al. 2014; Roth et al. 2010) need to be validated against well-documented case histories or physical model studies, which are currently lacking for stiff-uniyielding buried reservoir structures.

A series of centrifuge experiments were conducted at the University of Colorado, Boulder to evaluate the seismic performance of these shallow-buried reservoir structures. The structure stiffness, backfill soil type and slope, cover height, container type (rigid versus flexible boundaries), fixity conditions, and ground-motion characteristics were varied to evaluate their influence and relative importance on structural performance. The focus of this paper is on the influence of backfill soil type, soil cover, and backfill slope on the seismic performance of these stiff-uniyielding buried structures. A dry, cohesionless soil layer (Nevada sand) with and without cover as well as a compacted silty sand backfill (site-specific soil from Headworks reservoir construction site) that was either leveled or sloped, were used to evaluate the influence of structure embedment as well as backfill soil type and geometry. The model specimens were instrumented with accelerometers, linearly variable differential transformers (LVDTs), strain gauges, and tactile pressure transducers. The data from these instruments were used to calculate seismic lateral earth pressures, magnitude and location of dynamic lateral thrust, bending strain and moment distributions, and lateral deformations along the structure walls.

Background

The influence of shallow soil cover on the seismic response of underground box structures has not been evaluated experimentally in the past. Youd and Beckman (1996) studied the performance of reinforced highway box culverts during past earthquakes and showed that box culverts with a deeper fill cover experienced more damage due to increased inertial forces. Wang (1993) showed through a series of linear-elastic, finite-element analyses that a shallow soil cover similar to that considered in this study does not increase the racking of the structure significantly. Cilingir and Madabhushi (2011) experimentally and numerically studied the effect of embedment on the seismic response of relatively deeply buried (~2.5 and 6.5 m from soil surface to the top of structure), flexible box structures (flexibility ratios ranging from 14 to 330). They showed that larger seismic earth pressures are experienced on deeper tunnels. The influence of a shallow cover on seismic lateral earth pressures and bending moments has not been evaluated for stiffer box structures of interest (e.g., flexibility ratios ranging from about 0.1 to 2), which are important in design of critical buried reservoirs.

The effect of apparent cohesion induced by suction in the unsaturated backfill (Lu and Likos 2006) on seismic lateral earth pressures has previously been studied analytically, numerically, and experimentally. For example, analytical limit-state procedures have evaluated the effects of cohesion on dynamic earth pressures acting on yielding retaining walls (e.g., Okabe 1926; Chen and Liu 1990; Das 1996; Anderson et al. 2008). These studies showed that increasing cohesion leads to a significant decrease in dynamic earth pressures, assuming peak strength in the backfill soil and no change in the structure's stiffness, rotation, or translation.

Wilson (2009) performed numerical analyses of rigid retaining walls with compacted silty sand backfill and showed that rotation and wall translation have more influence on dynamic earth thrust than cohesion. Allowing for rotation and translation of the wall

significantly reduced seismic earth pressures, whereas adding cohesion reduced earth pressures only slightly. Numerical analyses by Candia and Sitar (2013) on braced basement walls and flexible cantilever walls retaining compacted low plasticity clay also showed that cohesion has a minor effect on dynamic earth pressures.

Wilson and Elgamal (2015) performed $1g$ shake table tests on short, rigid, retaining walls (1.7 m high) with a dense $c-\phi$ backfill material. They showed a similar distribution of lateral earth pressure as observed in prior analytical and numerical studies (e.g., Veletsos and Younan 1994; Psarropoulos et al. 2005; Davis 2003) where the dynamic increment of earth pressure increases toward the center and then decreases near the bottom for stiff retaining structures. Relatively low dynamic lateral earth pressures were recorded at smaller acceleration levels (less than $0.7g$), because of the high shear strength of the backfill soil including cohesion, which prevented a limit equilibrium type failure. Due to the deformation patterns in their retaining wall and the higher strength of the backfill soil, the lateral earth pressure time histories along the height of the wall were observed to be out of phase, which reduced the total applied force. At stronger accelerations, however, the lateral earth pressure distributions became more in phase, significantly amplifying the applied seismic force.

Realistic wave propagation, mean effective stress, and wall height cannot be properly simulated in $1g$ shake table tests. Therefore, Candia and Sitar (2013) and Mikola (2012) performed centrifuge experiments to evaluate the seismic response of braced basement walls and flexible cantilever walls retaining clean sand and low-plasticity clay with a relative compaction of 90% with respect to the standard Proctor compaction effort. They observed that the dynamic increment of pressure was affected by ground shaking intensity and wall displacement, but it was relatively independent of cohesion for free-field acceleration levels up to $\sim 0.6g$. They also observed that the dynamic lateral earth pressures acting on the basement walls increased linearly with depth. The basement struts did not prevent excessive bending of the walls in this case, which resulted in a more linear distribution of seismic earth pressures, as expected for more-flexible retaining structures (e.g., Hushmand et al. 2016). Furthermore, these experiments obtained earth pressures indirectly from strain gauges, which may increase the uncertainty.

In summary, a limited number of analytical, numerical, and experimental studies have been conducted on the influence of soil cover and cohesion on the seismic response of retaining and underground box structures. Previous studies have not evaluated the influence of backfill slope on the structure's seismic performance. The numerical simulations of the effect of soil cover presented in the literature focused primarily on the racking response and have not been validated sufficiently against physical model studies. Analytical, numerical, and experimental studies of the influence of cohesion of the surrounding soil on seismic lateral earth pressures involved different types of structures with different kinematic constraints, and accordingly led to results that did not always agree in terms of the magnitude and distribution of lateral earth pressures. Lastly, and importantly, the data available are limited for the seismic response of stiff-uniyielding buried box structures, which are of interest in the design of underground reservoir structures. Hence, the amplitude and distribution of seismic earth pressures on these underground structures in different types of soils are not well understood. Centrifuge modeling with adequate instrumentation can help evaluate SSI, deformations, and lateral earth pressures for this class of buried reservoir structures and the relative importance of different testing parameters on their seismic performance. Developing a fundamental understanding of these topics is a necessary step for the validation of advanced numerical tools before they can be used in design or parametric studies.

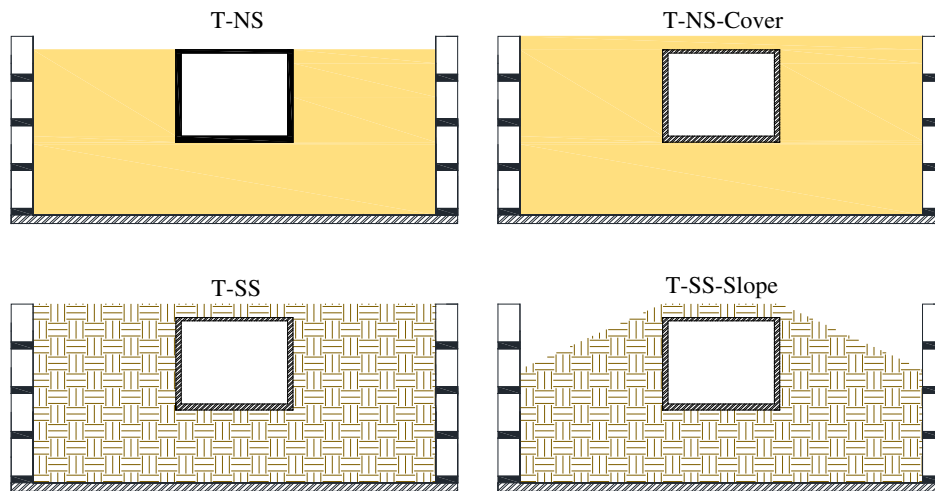


Fig. 1. Schematics of the centrifuge experiments to evaluate the influence of the properties and geometry of backfill soil

Centrifuge Experiments

A series of four centrifuge tests were conducted with the same structure, but different backfill soil properties and geometries, as shown schematically in Fig. 1. In this paper, the four experiments are referred to as T-NS (Nevada sand used as the backfill soil without a cover), T-NS-Cover (Nevada sand with a cover), T-SS (site-specific, compacted silty sand as the backfill soil with a cover), and T-SS-Slope (site-specific compacted silty sand with a cover and a 2:1 slope). The model specimens were prepared in a flexible shear beam (FSB) container to reduce boundary effects (Ghayoomi et al. 2013). The instrumentation layout of different tests is presented in Fig. 2. Experiments were performed at $60g$ of centrifugal acceleration using the large, $400g$ - t centrifuge at the University of Colorado, Boulder (Ko 1988). Earthquake motions were applied to the model specimens in flight using the servo-controlled, electrohydraulic shake table (Ketcham et al. 1991) mounted on the basket at the end of the centrifuge arm. A series of five earthquake motions were applied to the base of the models in the same sequence in the four experiments, followed by sinusoidal motions. All dimensions presented in this paper are in prototype scale, unless stated otherwise.

Soil Properties and Preparation

Experiments T-NS and T-NS-Cover were prepared with medium-dense, dry Nevada sand ($G_s = 2.65$; $e_{min} = 0.56$; $e_{max} = 0.84$; $D_{50} = 0.13$ mm; and $C_u = 1.67$) as backfill. In these tests, Nevada sand was pluviated from a predetermined height to achieve a relative density (D_r) of approximately 60% in T-NS. In T-NS-Cover, a 1.5-m (prototype scale) cover was added by pluviating a layer of Nevada sand over the specimen already used in T-NS after removing it from the centrifuge platform. Even though some densification of the Nevada sand layer in T-NS was expected after application of different motions, the densification inferred from LVDT measurements in T-NS indicate that it was roughly uniform across the container. Accordingly, it was deemed that the effects of soil cover could still be evaluated on the response of the underground structure in T-NS-Cover compared to T-NS, while keeping in mind the changes in the properties of the backfill soil due to densification and seismic history. Further, T-NS-Cover had similar backfill geometry and cover as T-SS, which enabled evaluating the influence of soil properties alone on the response of the buried structure.

Compacted, site-specific, silty sand obtained from the reservoir site in Los Angeles was used in T-SS and T-SS-Slope.

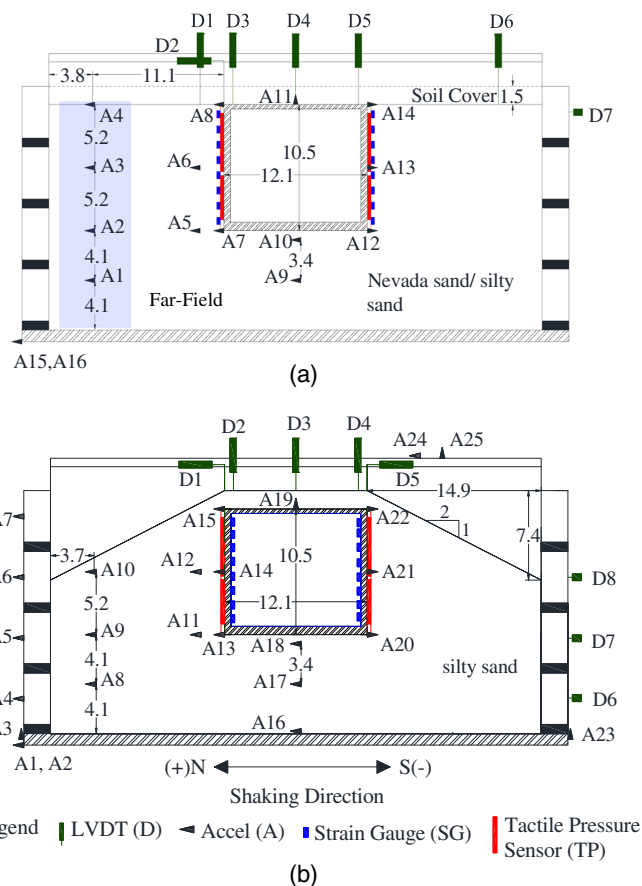


Fig. 2. Setup and instrumentation layout of centrifuge experiments: (a) T-NS, T-NS-Cover, and T-SS; (b) T-SS-Slope (dimensions are in prototype scale meters)

The site-specific soil that was used in the centrifuge experiments was first passed through a No. 40 sieve to remove large particles. The properties of the site-specific soil are summarized in Table 1, based on the gradation test [ASTM D422 (ASTM 2007a)], modified Proctor compaction test [ASTM D1557 (ASTM 2007b)], and direct shear test under consolidated drained conditions [ASTM D3080 (ASTM 2011)] performed by the authors.

Table 1. Mechanical Properties of Site-Specific, Compacted, Silty Sand Used in T-SS and T-SS-Slope

Unified soil classification system	Silty sand (SM)
Sand content	61.4%
Fines content	38.6%
Optimum water content	11.5%
Maximum dry unit weight	19.1 kN/m ³
Total unit weight	21.3 kN/m ³
Site-specific relative compaction	95%
Desired total unit weight	20.3 kN/m ³
Friction angle (peak)	32°
Cohesion (peak)	35 kPa

Note: Compaction corresponding to the modified proctor compaction effort.

The preparation of T-SS and T-SS-Slope took place in several steps. First, the soil was homogenized and the initial gravimetric content was measured to determine the amount of water to add to reach the optimum gravimetric water content of 11.5%. The soil was then moisture conditioned for 24 h. The moisture-conditioned soil was placed in several layers using specific lift heights and weights. It was subsequently compacted using a 44 N guided hammer to a certain volume to achieve the desired total unit weight of 20.3 kN/m³. Accelerometers were added to the model between soil layers at the locations shown in Fig. 2. The profiles in T-SS and T-NS-Cover were similar, only with different soil types. The model specimen in T-SS-Slope was prepared first in the same manner as T-SS, after which a flat spatula was used to cut the back-fill soil to a 2:1 downward slope on either side of the structure.

Structure Properties

The actual reservoirs are complex structures with many details that are difficult to scale and test in centrifuge. Hence, a simplified version of the reservoir was designed by maintaining a similar natural frequency and lateral stiffness as the designed prototype reservoir structure (Hushmand et al. 2014, 2016). The model structure was constructed of four pieces of welded 1018 Carbon Steel (density = 7,870 kg/m³ and Young's modulus = 2×10^8 kPa). Table 2 presents the dimensions, racking stiffness, and natural frequency of the structure used in the centrifuge experiments. Teflon polytetrafluorethylene (DuPont, Wilmington, Delaware) sheets were used on the container sides and ends of the structure to reduce friction at the structure–container interface. The test soil was glued to the base of the structure to provide a more realistic interface friction between the structure and the soil in each test.

Instrumentation

Data was acquired using accelerometers, LVDTs, strain gauges, and tactile pressure sensors, as shown in Fig. 2 (Tekscan 2003).

Table 2. Dimensions and Properties of Model Underground Structure

Dimension or property	Value in prototype scale
Height and width (m) outer to outer	10.5 and 12.1
Thickness	
Base (mm)	688
Roof (mm)	371
Walls (mm)	558
Lateral stiffness, K_s (kN/m/m)	31,500
Fundamental frequency (Hz)	
Numerical	4
Experimental	3.9

Accelerometers were placed horizontally at the container base, on the container frames, at different elevations within the soil in the far-field, adjacent to the buried structure, on the structure, and on the instrumentation rack to monitor movement. Vertical accelerometers were similarly placed at the container base, roof of the structure, and instrumentation rack. LVDTs were used to measure the settlement of soil and structure, the lateral displacement of the structure, lateral displacement of FSB container frames, and lateral movement of container base. Eight strain gauges were installed on each wall of the structure (total of 16) to measure bending strains and hence, bending moments. Four tactile pressure sensors were used to measure total pressure directly on both sides of the structures. Tactile sensors were equilibrated, conditioned, and statically and dynamically calibrated prior to use in the centrifuge, following the procedure recommended by Dashti et al. (2012), Gillis et al. (2015), and El Ganainy et al. (2014).

Ground Motions

A series of earthquake motions were selected with a range of amplitudes, frequency contents, and durations and applied during T-NS, T-NS-Cover, T-SS, and T-SS-Slope. These motions included scaled versions of the horizontal acceleration recordings at the Sylmar Converter Station during the 1994 Northridge Earthquake (NSC52), the Los Gatos Presentation Center (LGPC) Station during the 1989 Loma Prieta Earthquake (LGP000), and the Istanbul Station during the 1999 Izmit Earthquake in Turkey (IST180), all obtained from the Pacific Earthquake Engineering Research (PEER) database (Ancheta et al. 2013). Sinusoidal motions were also applied in these tests, which are not presented in this paper. The achieved base motions in the centrifuge are referred to as Northridge-L (low intensity), Northridge-M (medium intensity), Northridge-H (high intensity), Izmit, and Loma. The properties of the achieved base motions in T-NS are presented in Table 3.

A small degree of variation in the base motions among different tests was expected due to the change in weight and natural frequency of the model specimen as well as inconsistencies of the shake table. The spectral acceleration (5% damped) of the achieved base motions in T-NS, T-NS-Cover, T-SS, and T-SS-Slope are compared in Fig. 3, showing a reasonable comparison, particularly for weaker motions. More variation was observed during stronger motions (e.g., Northridge-H and Loma) at higher frequencies that are more difficult for the shake table to control and reproduce.

Experimental Results

Acceleration Response

The influence of backfill soil type and geometry was evaluated on soil–structure interaction effects (both inertial and kinematic) near the underground structure through spectral ratios of structure to far-field accelerations in the four experiments. Fig. 4 shows the

Table 3. Base Earthquake Motion Properties as Recorded during T-NS by Accelerometer A15 (All Units in Prototype Scale)

Motion name	PGA (g)	Arias intensity I_a (m/s)	Significant duration D_{5-95} (s)	Mean frequency f_m (Hz)	Predominant frequency f_p (Hz)
Northridge-L	0.36	1.6	15.4	1.4	2.9
Northridge-M	0.81	5.4	19.5	1.5	3.6
Northridge-H	1.2	11.6	25.1	1.6	3.6
Izmit	0.33	2.1	39.5	1.8	4.2
Loma	1.0	12.4	13.3	2.0	3.7

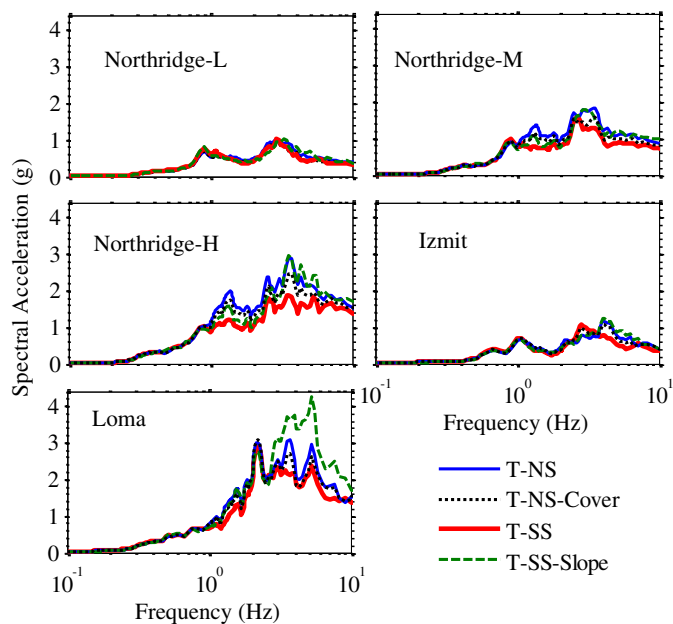


Fig. 3. Comparison of the recorded base motion spectral accelerations (5% damped) in T-NS, T-NS-Cover, T-SS, and T-SS-Slope

spectral ratios of accelerations at the bottom, middle, and top of the structure to those in the far-field in each test during three representative ground motions (Northridge L, M, and H). These ratios provide insight into whether accelerations were amplified or deamplified on the structure compared to the far-field recordings that approximate one-dimensional (1D) free-field site response. Due to a lack of 1D far-field conditions in T-SS-Slope, the spectral ratios are not presented for this experiment.

The structure to far-field spectral ratios increased at shallower depths in T-NS and T-NS-Cover. As the confining pressure

increased, the movement of the buried structure was controlled more by the surrounding soil. The highest amplification of spectral ratios was observed at the top of the structure near the predominant frequency of the motion ($f_p \approx 3$ Hz). The added cover and stiffness of the backfill soil slightly reduced the degree of amplification in structural accelerations during T-NS-Cover compared to T-NS.

The properties of the backfill soil significantly influenced the accelerations on the structure. For example, when Nevada sand was replaced with the site-specific, compacted silty sand in T-SS, no noticeable change was observed in accelerations recorded on the structure compared to the far-field at any depth (e.g., spectral ratios of near 1.0). It appeared that the structure closely followed the movement of the compacted silty sand at all depths during this test. In all experiments, however, the impact of structural inertia on accelerations appeared to be minor, as no particular amplification was observed near the structure's fundamental frequency of 4 Hz.

Racking Displacements

Racking is defined as the lateral displacement of the roof of the box structure relative to its base. The racking displacement is often used in design to evaluate peak bending moments in a simple frame analysis of the two-dimensional (2D) box structure. In practice, the peak transverse racking of a box structure is often estimated with respect to that in the free-field using the National Cooperative Highway Research Program (NCHRP) 611 guideline (Anderson et al. 2008). The NCHRP 611 guideline is, however, based on the results of dynamic finite-element analyses performed by Wang (1993) on buried box structures. The centrifuge results presented in this paper enable an experimental evaluation of the applicability of this guideline to stiff-uniyielding, underground reservoir structures with varying backfill soil and geometry.

Lateral displacement time histories were obtained by double integrating and baseline correcting the accelerometer recordings. Racking (Δ) was then calculated as the difference in lateral displacements at the top and bottom of the structure ($\Delta_{\text{structure}}$) and

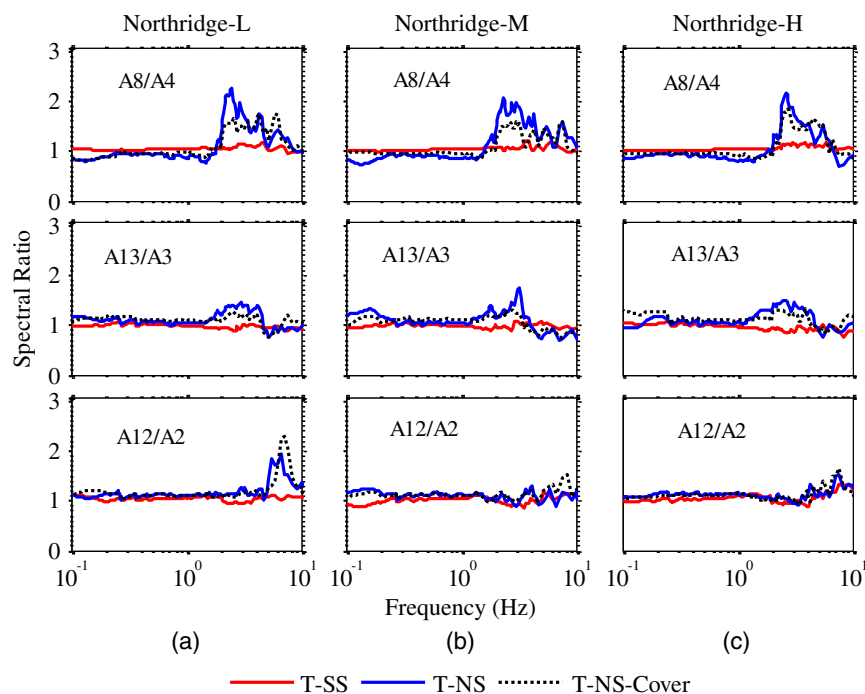


Fig. 4. Spectral ratio (5% damped) of structure to far-field accelerations in three tests (T-NS, T-NS-Cover, and T-SS) during the Northridge-L, Northridge-M, and Northridge-H motions at the top, middle, and bottom of the structure wall

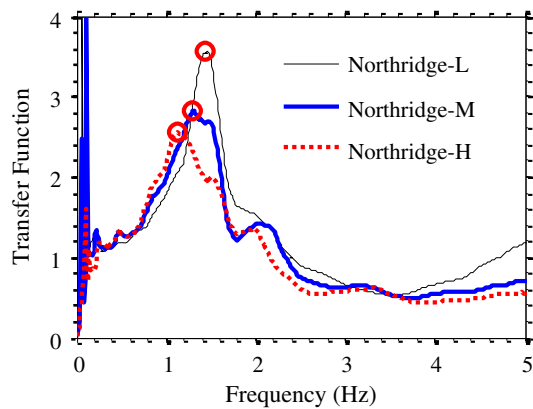


Fig. 5. Transfer function of surface to base accelerations in the far-field in T-SS during the Northridge-L, Northridge-M, and Northridge-H motions to determine the strain-compatible fundamental frequency and shear modulus of the soil column away from the structure

in the far-field at the same elevations (Δ_{FF}). The peak values of racking displacement on the structure ($\max|\Delta_{structure}|$) and far-field soil ($\max|\Delta_{FF}|$) were subsequently used to obtain the racking ratio ($R = \max|\Delta_{structure}|/\max|\Delta_{FF}|$) during each test and motion. Since there was no location in T-SS-Slope approximating 1D free-field conditions, the far-field response in T-SS was used instead to obtain the racking ratios in T-SS-Slope. Even though the achieved base motions were slightly different in the two experiments, particularly during stronger motions, this comparison was still insightful.

To calculate the flexibility of the structure relative to the far-field in accordance with the NCHRP 611 guidelines, the flexibility ratio, $F = (G_m \cdot B)/(K_s \cdot H)$, needed to be calculated, where G_m is defined as the mean strain-compatible shear modulus of soil in the free-field, B is the structure width, K_s is the racking stiffness of the structure, and H is its height (Anderson et al. 2008). Table 2 summarizes the properties of the structure used in centrifuge testing. The G_m of soil was experimentally obtained by calculating the effective fundamental frequency (f'_{so}) of the far-field soil from the transfer function of accelerations at the surface with respect to base during a given motion (e.g., Fig. 5). The strain-compatible, average shear wave velocity of the far-field soil, was computed as $\bar{V}'_s = 4H \times f'_{so}$, and the strain-compatible G_m of soil as $G_m = \rho \bar{V}'_s{}^2$, where H is the height of the far-field soil column and ρ is the soil's mass density in a given test. As expected, the f'_{so} of the far-field soil in T-SS was observed in Fig. 5 to decrease with stronger shaking due to softening.

The experimentally obtained values of racking versus flexibility ratio (R versus F) in all four tests during all motions are compared with the numerically obtained values from the NCHRP 611 guideline, shown in Fig. 6. In general, the results compared well, although the experimental values of R were often slightly greater than those from the NCHRP guideline. Both R and F values increased slightly in T-NS-Cover compared to T-NS. This trend was likely due to the increase in soil stiffness (and hence, flexibility ratio or F) in T-NS-Cover compared to T-NS after the application of many motions and soil densification, in addition to the possible effect of the inertia of the soil cover. The impact of a shallow soil cover alone on racking ratios is not clear from these experiments, but previous numerical observations by Wang (1993) have shown a minor influence.

The use of a compacted silty sand backfill soil in T-SS increased G_m to a value closer to the structure's racking stiffness in this case (e.g., $F \approx 1$). Therefore, the structure underwent racking deformations that were similar to those in the far-field soil (i.e., $R \approx 1$).

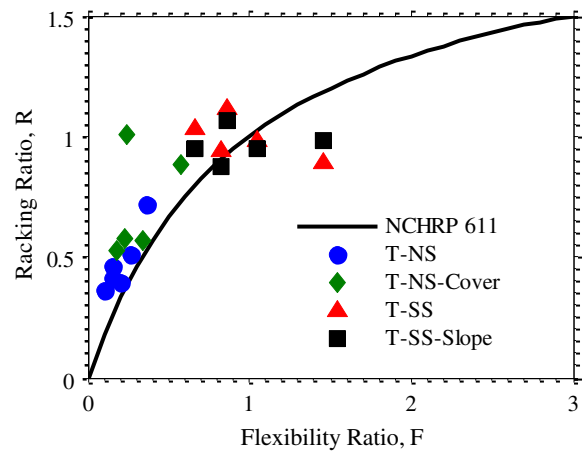


Fig. 6. Experimental racking versus flexibility ratios of the underground reservoir structure during different ground motions and tests as compared to the NCHRP 611 guideline

A similar trend was observed previously in the acceleration response of structure and far-field soil in T-SS. The addition of the slope in T-SS-Slope did not noticeably change R versus F values compared to T-SS. Further, the change in ground motion intensity did not alter R significantly during the tests with site-specific backfill soil, as in all cases the structure was observed to primarily follow the deformation of the backfill soil.

Seismic Lateral Earth Pressures

The dynamic increment of pressure ($\Delta\sigma_E$) was estimated as the difference between total and preshake, static lateral earth pressure recordings. To reduce scatter, the data obtained from nine sensels were averaged to represent a larger pressure area after removing the nonworking sensels (Hushmand et al. 2016). Then, the pressure time histories were averaged over the corresponding row of sensels to obtain one time history at a given depth. This method was successful in reducing the scatter in pressure recordings, particularly when in contact with granular materials with local inhomogeneities (Gillis et al. 2015).

The dynamic increment of thrust was estimated by numerically integrating the dynamic pressure profile along the wall at each instance of time, using the trapezoidal rule. The resulting dynamic thrust time histories during the Northridge-L motion are compared among the four tests in Fig. 7 along with the acceleration time history of the corresponding base motion. The presented thrust time histories were subject to a band-pass, fifth-order, acausal Butterworth filter with corner frequencies of 0.1 and 15 Hz, to remove low-frequency and high-frequency noise that was sometimes present in the tactile sensor record and could affect the estimated peak dynamic thrust. As a result of filtering, however, the permanent change in thrust that is typically expected cannot be obtained from this figure, but the transient thrust may be compared among the four tests.

The Fourier amplitude spectra (FAS) of dynamic thrust are compared to those of acceleration at the base of the buried structure wall in Fig. 8 during the Northridge-L motion in all four tests. The frequency content of dynamic thrust was often roughly similar to its base acceleration. The acceleration and dynamic thrust on the buried structure are both expected to be influenced by site response, structure's fixity, stiffness of the structure relative to soil, and height of the structure relative to the propagating wavelength, as well as structural inertia. Therefore, the similarity between their frequency contents was expected. Significant energy was present in both

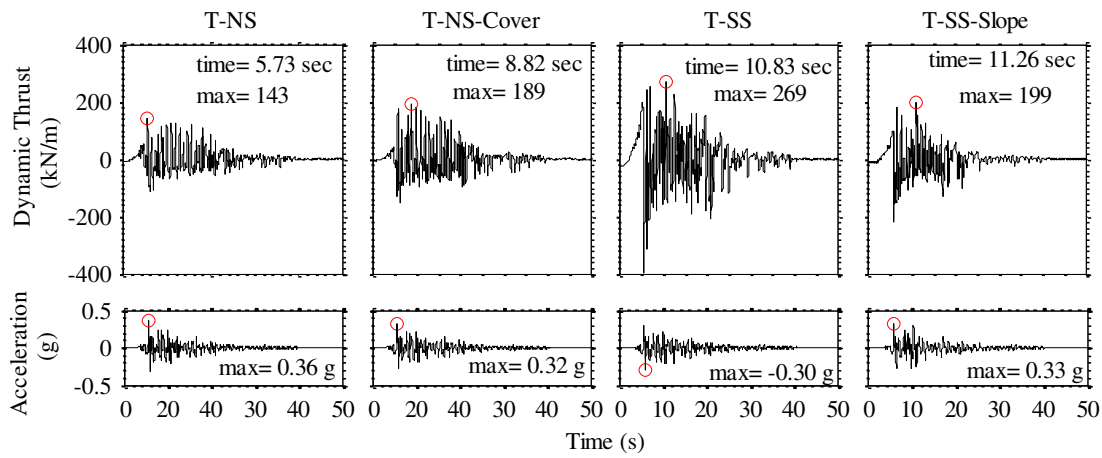


Fig. 7. Dynamic thrust time histories on the structures in T-NS, T-NS-Cover, T-SS, and T-SS-Slope during the Northridge-L motion

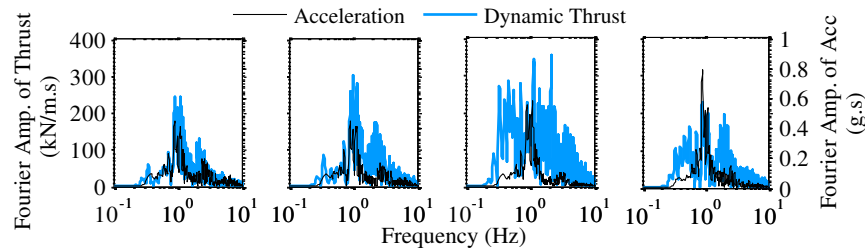


Fig. 8. Fourier amplitude spectra of dynamic thrust and structure base acceleration in T-NS, T-NS-Cover, T-SS, and T-SS-Slope during the Northridge-L motion

dynamic thrust and acceleration near 1–1.5 Hz in all experiments, which corresponded to the effective, strain-dependent, fundamental frequency of the site during the corresponding motion ($f_{so} \approx 1.2$ Hz in T-NS, $f_{so} \approx 1.4$ Hz in T-NS-Cover, and $f_{so} \approx 1.5$ Hz in T-SS, corresponding to effective average shear wave velocities, $V_s^i = 4 \cdot f_{so} \cdot H_{site} \approx 90, 113,$ and 121 m/s in T-NS, T-NS-Cover, and T-SS, respectively during Northridge-L). This observation points to the critical influence of site response and resonance on seismic earth pressures experienced by the buried structure. Further, a noticeable content in dynamic thrust was observed near 2.2–2.5 Hz. This content may have been related to kinematic interaction. The wavelength (λ) associated with these frequencies ranged from approximately 36 to 55 m. The corresponding wavelength to structure height ratio ($\lambda/H_{structure}$) ranged from 3 to 5, which was near the peak influence of kinematic interaction on seismic earth thrust, as shown analytically by Brandenberg et al. (2015).

The influence of structural inertia on its accelerations or seismic lateral earth pressures was likely minor in these tests, as no significant amplifications were observed near the fundamental frequency of 4 Hz. This was also confirmed in Fig. 4 when comparing the acceleration of the structure with far-field soil. Nevertheless, the effect of structural inertia may be important for other conditions. Future numerical studies, in which different effects can be properly isolated, can provide valuable insights into the potential influence of structural inertia and conditions at which it may play an important role.

The $\Delta\sigma_E$ profile at the time of maximum thrust is shown in Fig. 9 in all four tests during all earthquake motions. A third-order polynomial was fit to the $\Delta\sigma_E$ distribution at the time of maximum thrust to estimate the centroid location and to interpret the

magnitude and trends despite the scatter present in the recordings. The centroid of $\Delta\sigma_E$ at the time of maximum thrust in all four tests versus the peak ground acceleration (PGA) of the far-field surface motion (A4) is shown in Fig. 10, which was obtained from the polynomial fit. For all the conditions investigated here, the $\Delta\sigma_E$ increased towards the center of the wall and decreased near the top and bottom of the wall. These distributions were more consistent with those predicted analytically, numerically, and experimentally for stiffer structures in different soils (e.g., Veletsos and Younan 1994; Psarropoulos et al. 2005; Richards et al. 1999; Davis 2003; Gazetas et al. 2004; Psarropoulos et al. 2005; Wilson 2009; Wilson and Elgamal 2015) than those observed experimentally and numerically for more flexible structures (e.g., Mikola 2012; Candia and Sitar 2013). The differences observed in the distribution of dynamic earth pressures, therefore, are mainly due to the differences in kinematic constraints and flexural rigidity of the wall system employed rather than the stiffness and strength of the backfill soil.

The backfill soil type and geometry also influence the shape and magnitude of $\Delta\sigma_E$ profiles. The addition of a shallow soil cover as well as the increase in backfill soil stiffness during T-NS-Cover slightly increased the dynamic pressures near the top of the wall and shifted the centroid upward when compared to T-NS during stronger motions. The additional apparent cohesion and stiffness of the site-specific, compacted soil in T-SS also slightly altered the distribution of $\Delta\sigma_E$ when compared with T-NS-Cover of the same backfill geometry: $\Delta\sigma_E$ was often observed to increase slightly near the center and decrease near the top and bottom of the wall in T-SS compared to the responses observed in the T-NS-Cover. A review of the pressure time histories along the wall indicated that $\Delta\sigma_E$ time histories were primarily in phase in T-NS-Cover but not in T-SS. This means that when $\Delta\sigma_E$ peaked near the

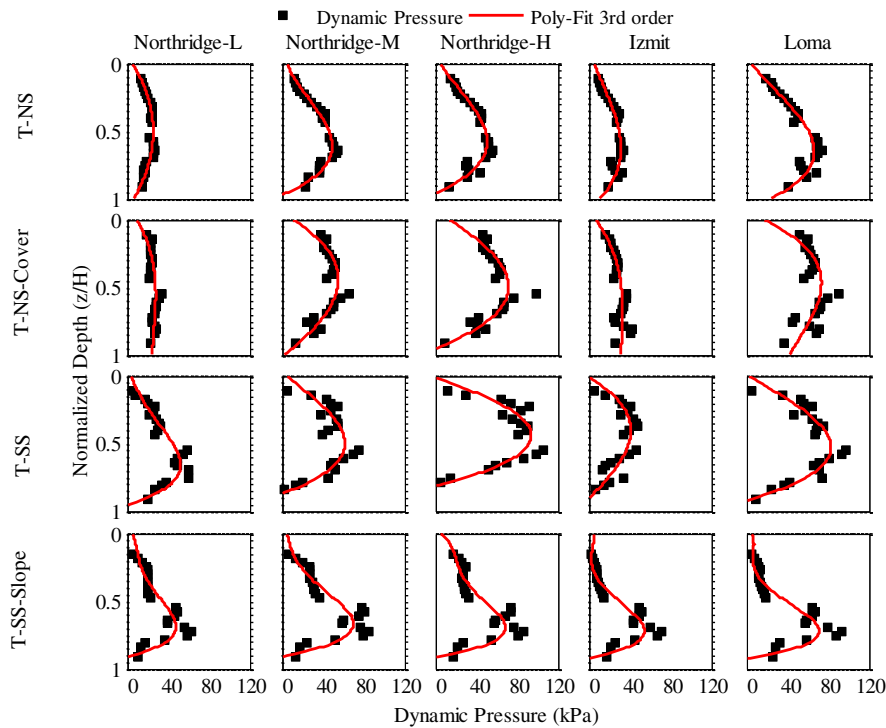


Fig. 9. Dynamic pressure ($\Delta\sigma_E$) profiles at the time of maximum thrust measured by tactile pressure sensors in T-NS, T-NS-Cover, T-SS, and T-SS-Slope during different earthquake motions

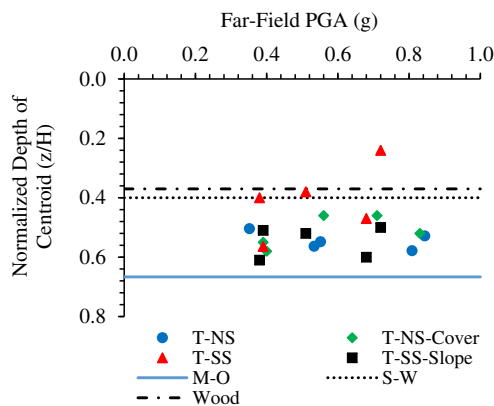


Fig. 10. Centroid of $\Delta\sigma_E$ at the time of maximum thrust as a function of far-field surface PGA in four centrifuge tests compared with analytical procedures of Mononobe-Okabe, Seed-Whitman, and Wood

center, it approached its minimum near the top and bottom of the wall in T-SS during the motions investigated. This observation is consistent with those of Wilson and Elgamal (2015) for a rigid retaining wall with compacted $c - \phi$ backfill soil at lower levels of shaking, when a limit equilibrium failure state is not expected. When comparing the dynamic thrust, which averages the $\Delta\sigma_E$ distribution along the height of the wall, no significant and consistent difference was observed between T-NS-Cover and T-SS. Therefore, similar to other experimental and numerical observations (e.g., Wilson 2009; Wilson and Elgamal 2015; Candia and Sitar 2013), cohesion of the backfill soil was observed to have a relatively minor effect on seismic earth thrust regardless of the kinematic constraint or flexural rigidity of the wall employed. The centroid of the $\Delta\sigma_E$ profile, however, appeared to move upward

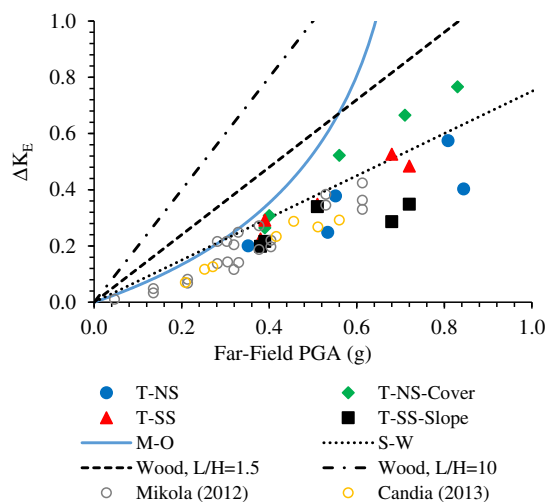


Fig. 11. Dynamic coefficient of lateral earth pressure (ΔK_E) at the time of maximum thrust as a function of far-field surface PGA in four centrifuge tests compared with analytical procedures of Mononobe-Okabe, Seed-Whitman, and Wood and previous centrifuge experiments performed by Mikola (2012) and Candia and Sitar (2013) on a basement wall

slightly in T-SS compared to T-NS-Cover, particularly during stronger motions. The $\Delta\sigma_E$ values reduced near the top of the wall in T-SS-Slope compared to T-SS, because of the reduction in soil mass and inertia near the surface due to the sloped backfill, as expected.

The dynamic coefficient of lateral earth pressure (ΔK_E) was calculated for an equivalent triangular dynamic lateral earth pressure profile by dividing the actual dynamic thrust by $\gamma H^2/2$, where γ is the total unit weight of the corresponding backfill soil and H the

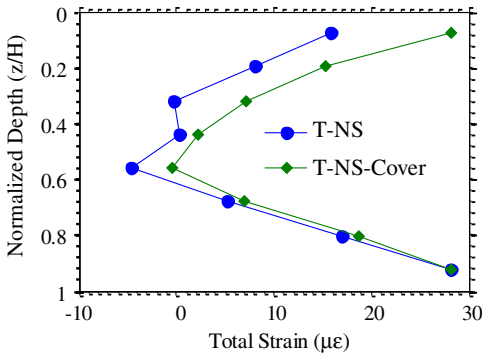


Fig. 12. Effect of soil cover on static bending strains on the walls of the underground structure comparing T-NS and T-NS-Cover

wall height. ΔK_E , as originally introduced by Seed and Whitman (1970), was based on a triangular distribution of dynamic lateral earth pressures, while the dynamic lateral earth pressure profiles in these experiments resembled a parabolic shape. The equivalent ΔK_E values calculated based on experimental recordings of pressure were used to compare the magnitude of seismic force among the different experiments, previous centrifuge tests, and available simplified procedures. The equivalent ΔK_E values obtained experimentally at the time of maximum thrust as a function of the PGA of the far-field surface motion (A4) are shown in Fig. 11. This figure also includes the results obtained from previous centrifuge experiments performed (1) by Mikola (2012) on a model basement structure retaining a cohesionless soil, (2) by Candia and Sitar (2013) on a basement structure retaining a cohesive soil (both reported at the time of maximum moment), and (3) predictions from the M-O, S-W, and Wood methods for comparison.

The ΔK_E values obtained in all experiments generally increased with increasing shaking intensity and were often smaller than those

predicted by the S-W procedure. However, the ΔK_E values were larger than S-W during T-NS-Cover, particularly for PGA values greater than about 0.4, possibly due to the added stiffness and confining pressure in the backfill soil. Strong motions with large PGA's are common in the design of buried reservoir structures, since they are considered as a critical component of the lifeline infrastructure. The addition of the soil cover and backfill soil stiffness in T-NS-Cover appeared to have increased the magnitude of dynamic earth pressures compared to T-NS. Even though the magnitude of seismic earth pressures and thrust was not significantly different in T-SS and T-NS-Cover in most cases, ΔK_E was smaller in T-SS due to compaction that increased soil's total unit weight. The reliability of pressure sensors, however, is a topic of ongoing research, and therefore it is important to also evaluate bending moments (obtained from strain gauges) in parallel, which are affected by seismic lateral earth pressures and wall inertia simultaneously.

Bending Strains and Moments

Bending strains were measured on both walls during all four tests with strain gauges. Static bending strains increased near the top of the buried structure when soil cover was added in T-NS-Cover compared to T-NS, as shown in Fig. 12. Tensile surface strain due to bending (i.e., wall curvature outward) is shown as positive in this figure. Strain gauge recordings during earthquake loading did not indicate any permanent change in strains for the type of structures evaluated in this study. The dynamic increment of bending moment (ΔM_E) along the wall was subsequently calculated from the corresponding strain values, as shown in Fig. 13. The tactile sensors had a separate data acquisition system from other sensors. Therefore, to avoid possible errors associated with time synchronization of responses, dynamic moments (ΔM_E) are reported at the time of maximum moment as opposed to maximum thrust obtained from tactile sensors.

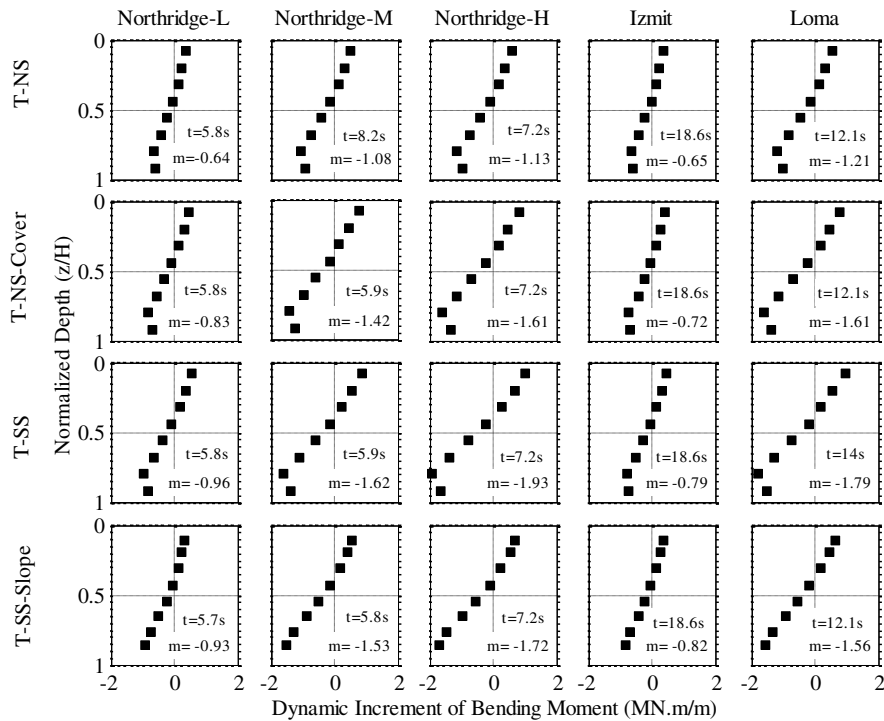


Fig. 13. Dynamic increment of bending moments (ΔM_E) on the south wall of tests T-NS, T-NS-Cover, T-SS, and T-SS-Slope at the time of maximum moment during different motions

The shape of the ΔM_E profile along the wall was roughly linear in the four tests during all motions, with its peaks near the fixed connections with the roof and base of the reservoir structure. The magnitude of ΔM_E increased slightly from T-NS to T-NS-Cover, with the added overburden of the soil cover and the increased stiffness of the backfill soil. The change in soil properties did not significantly change ΔM_E in T-SS compared to T-NS-Cover. There was, however, a slight reduction in ΔM_E from T-SS to T-SS-Slope near the top of the wall due to the presence of a sloped backfill, as expected, due to reduce mass near the top. These trends were consistent with those of $\Delta\sigma_E$.

Conclusion

Dynamic centrifuge tests were performed on stiff-unchanging, buried reservoir structures to consider the influences of soil cover, backfill soil type, and a sloped backfill on soil–structure interaction, racking deformations, seismic lateral earth pressures, and bending strains and moments in the structure. The primary conclusions of this paper are as follows:

1. In experiments involving dry, medium-dense Nevada sand, accelerations were amplified on the buried structure compared to the far-field soil at shallow depths near the predominant frequency of the base motion. Adding the soil cover and stiffness reduced the independent movement of the structure and hence the amplification of accelerations compared to the far-field soil. The compacted, site-specific, silty sand backfill with a similar cover further limited the independent movement of the buried structure due to soil's greater stiffness, where the structure accelerations primarily followed those of the far-field soil.
2. The increased backfill soil stiffness and flexibility ratio after subsequent shaking together with an added shallow soil cover increased the structure's racking response slightly. Using a compacted, partially saturated backfill increased the soil's stiffness further to a value near the racking stiffness of the structure in this case (i.e., $F \approx 1$). Hence, the structure's racking deformation approached that of the far-field soil (i.e., $R \approx 1$). The addition of a sloped backfill did not significantly affect the racking and flexibility ratios compared to the case without a slope.
3. The frequency content of dynamic thrust on the walls of the buried structure was often roughly similar to its acceleration, because they were both affected by site response as well as structure's fixity, stiffness relative to soil, and inertia. Both dynamic thrust and acceleration showed a peak near the effective fundamental frequency of the site, pointing to the critical importance of site response on seismic earth pressures. Kinematic interaction also influenced the observed dynamic thrust where the wavelength to structure height ratio ($\lambda/H_{\text{structure}}$) ranged from approximately 3 to 5. The impact of structural inertia alone on its response was likely minor during these experiments.
4. The addition of a shallow soil cover slightly increased seismic earth pressures ($\Delta\sigma_E$) on the structure near its roof. The additional density, stiffness, and apparent cohesion of the site-specific, compacted silty sand slightly increased $\Delta\sigma_E$ near the center and decreased $\Delta\sigma_E$ near the roof and base of the structure. The increased strength of the backfill soil led to a phase difference in $\Delta\sigma_E$ time histories along the height of the wall (i.e., when $\Delta\sigma_E$ peaked near the center, it approached lower values near the top and bottom). But, the additional soil stiffness and apparent cohesion did not have a significant influence on seismic earth thrust, which averages the $\Delta\sigma_E$ distribution along the wall, while it shifted its centroid upward slightly. These results combined with previous studies indicate that soil cohesion

has a minor effect on seismic earth thrust, regardless of the kinematic constraints or flexural rigidity of the wall. The sloped backfill caused the dynamic lateral earth pressures to decrease near the top and its centroid to move downward, because of the reduction in soil mass and inertia near the surface.

5. The trends in dynamic bending moments acting on structure walls (ΔM_E) were in line with those of $\Delta\sigma_E$. The addition of a soil cover and backfill soil stiffness increased the magnitude of ΔM_E , particularly near the bottom of the wall. The change in soil properties in the site-specific soil did not significantly affect the magnitude of ΔM_E , but increased it slightly near the bottom of the wall. The sloped backfill, on the other hand, decreased ΔM_E near the top of the wall because of less confinement.

The methods commonly used to evaluate the response of underground and retaining structures in terms of deformation, magnitude and distribution of seismic earth pressures, and bending moments do not adequately consider the range of backfill soil properties, flexural stiffness, kinematic constraints, and ground motions for which critical underground reservoir facilities must be designed. The experimental results presented in this paper are intended to provide important insights into the influence of backfill soil on the seismic performance of a class of stiff-unchanging buried structures with translational and rotational restraints at the top and bottom. Parallel nonlinear numerical simulations with additional variations are, however, necessary and underway before the results can be used to provide general recommendations for practice.

Acknowledgments

The authors would like to thank the Los Angeles Department of Water and Power (LADWP) for financial support of this research. They would also like to thank Drs. Min Zhang and Majid Ghayoomi for their support in the planning and execution of the centrifuge experiments.

References

- Ancheta, T. D., et al. (2013). "PEER NGA-West 2 database." *PEER Rep. 2013/03*, Pacific Earthquake Engineering Research Center, Univ. of California, Berkeley, CA.
- Anderson, D. G., Martin, G. R., Lam, I. P., and Wang, J. N. (2008). "Seismic design and analysis of retaining walls, buried structures, slopes and embankments." *NCHRP Rep. 611*, Transportation Research Board, National Cooperative Highway Research Program, Washington, DC.
- ASTM. (2007a). "Standard test method for particle-size analysis of soils." *ASTM D422*, West Conshohocken, PA.
- ASTM. (2007b). "Standard test methods for laboratory compaction characteristics of soil using modified effort." *ASTM D1557*, West Conshohocken, PA.
- ASTM. (2011). "Standard test method for direct shear test of soils under consolidated drained conditions." *ASTM D3080*, West Conshohocken, PA.
- Brandenberg, S. J., Mylonakis, G., and Stewart, J. P. (2015). "Kinematic framework for evaluating seismic earth pressures on retaining walls." *J. Geotech. Geoenviron. Eng.*, [10.1061/\(ASCE\)GT.1943-5606.0001312](https://doi.org/10.1061/(ASCE)GT.1943-5606.0001312), 04015031.
- Candia, G., and Sitar, N. (2013). "Seismic earth pressures on retaining structures in cohesive soils." California Dept. of Transportation, Univ. of California Berkeley, Berkeley, CA.
- Chen, W. F., and Liu, X. L. (1990). *Limit analysis in soil mechanics*, Elsevier, Amsterdam, Netherlands.
- Cilingir, U., and Madabhushi, S. G. (2011). "Effect of depth on the seismic response of square tunnels." *Soils Found.*, *51*(3), 449–457.

- Das, B. M., and Puri, V. K. (1996). "Static and dynamic active earth pressure." *Geotech. Geol. Eng.*, 14(4), 353–366.
- Dashti, S., Gillis, K., Ghayoomi, M., and Hashash, Y. (2012). "Sensing of lateral seismic earth pressures in geotechnical centrifuge modeling." *Proc., 15th World Conf. on Earthquake Engineering*, Sociedade Portuguesa de Engenharia Sísmica (SPES), Lisbon, Portugal, 1–10.
- Davis, C. A. (2003). "Lateral seismic pressures for design of rigid underground lifeline structures." *Proc., 6th U.S. Conf. on Lifeline Earthquake Engineering*, ASCE, Reston, VA, 1001–1010.
- El Ganainy, H., Tessari, A., Abdoun, T., and Sasanakul, I. (2014). "Tactile pressure sensors in centrifuge testing." *Geotech. Test. J.*, 37(1), 1–13.
- Gazetas, G., Psarropoulos, P. N., Anastasopoulos, I., and Gerolymos, N. (2004). "Seismic behavior of flexible retaining systems subjected to short-duration moderately strong excitation." *Soil Dyn. Earthquake Eng.*, 24(7), 537–550.
- Ghayoomi, M., Dashti, S., and McCartney, J. S. (2013). "Performance of a transparent flexible shear beam container for geotechnical centrifuge modeling of dynamic problems." *Soil Dyn. Earthquake Eng.*, 53(10), 230–239.
- Gillis, K., Dashti, S., and Hashash, Y. (2015). "Dynamic calibration of tactile sensors for measurement of soil pressures in centrifuge." *ASTM Geotech. Test. J.*, 38(3), 261–274.
- Harounian, A., Davis, C. A., Lew, M., and Hudson, M. B. (2014). "Beyond code-based design: Use of advanced numerical modeling to support design of Los Angeles's headworks reservoir." *Proc., 2014 Geo-Congress*, ASCE, Reston, VA, 3044–3053.
- Hushmand, A., et al. (2014). "Seismic soil-structure interaction and lateral earth pressures on buried reservoir structure." *Proc., GeoCongress 2014 (GSP 234)*, ASCE, Reston, VA, 1215–1224.
- Hushmand, A., et al. (2016). "Seismic performance of underground reservoir structures: Insight from centrifuge modeling on the influence of structure stiffness." *J. Geotech. Geoenviron. Eng.*, 10.1061/(ASCE)GT.1943-5606.0001477, 04016020.
- Ketcham, S. A., Ko, H. Y., and Sture, S. (1991). "Performance of an earthquake motion simulator for a small geotechnical centrifuge." *Centrifuge 91*, H. Y. Ko and F. G. McLean, eds., Balkema, Rotterdam, Netherlands, 361–368.
- Ko, H. Y. (1988). "The Colorado centrifuge facility." *Centrifuge 88*, J. F. Corte, ed., Balkema, Rotterdam, Netherlands, 73–75.
- Lu, N., and Likos, W. J. (2006). "Suction stress characteristic curve for unsaturated soil." *J. Geotech. Geoenviron. Eng.*, 10.1061/(ASCE)1090-0241(2006)132:2(131), 131–142.
- Mikola, R. (2012). "Seismic earth pressures on retaining structures and basement walls in cohesionless soils." Ph.D. thesis, Univ. of California, Berkeley, CA.
- Mononobe, N., and Matsuo, M. (1929). "On the determination of earth pressures during earthquakes." *Proc., World Engineering Congress*, Vol. 9, Engineering Society of Japan, Tokyo, 179–187.
- Okabe, S. (1926). "General theory of earth pressure." *J. Jpn. Soc. Civ. Eng.*, 12(1), 311.
- Psarropoulos, P. N., Klonaris, G., and Gazetas, G. (2005). "Seismic earth pressures on rigid and flexible retaining walls." *Int. J. Soil Dyn. Earthquake Eng.*, 25(7), 795–809.
- Richards, R., Huang, C., and Fishman, K. L. (1999). "Seismic earth pressure on retaining structures." *J. Geotech. Geoenviron. Eng.*, 125(9), 771–778.
- Roth, W. H., Mehra, M., Su, B., and Davis, C. A. (2010). "The meaning of seismic earth pressure." *Annual SEAOC Convention*, Association of California, Structural Engineers Association of California, Sacramento, CA, 511–522.
- Seed, H. B., and Whitman, R. V. (1970). "Design of earth retaining structures for dynamic loads." *ASCE Specialty Conf., Lateral Stresses in the Ground and Design of Earth Retaining Structures*, ASCE, New York, 103–147.
- Tekscan. (2003). "Tekscan I-scan equilibration and calibration practical suggestions." South Boston.
- Veletos, A. S., and Younan, A. H. (1994). "Dynamic modeling and response of soil-wall systems." *J. Geogr. Eng.*, 120(12), 2155–2179.
- Wang, J. N. (1993). *Seismic design of tunnels: A state-of-the-art approach*, Parsons Brinckerhoff Quade & Douglas, Inc, New York.
- Wilson, P. (2009). "Large scale passive force-displacement and dynamic earth pressure experiments and simulations." Ph.D. thesis, Univ. of California, San Diego.
- Wilson, P., and Elgamal, A. (2015). "Shake table lateral earth pressure testing with dense $c-\phi$ backfill." *Soil Dyn. Earthquake Eng.*, 71, 13–26.
- Wood, J. H. (1973). "Earthquake induced soil pressures on structures." Ph.D. thesis, California Institute of Technology, Pasadena, CA.
- Youd, T. L., and Beckman, C. J. (1996). "Highway culvert performance during past earthquakes." *Rep. No. NCEER-96-0015*, National Center for Earthquake Engineering Research, Buffalo, NY.
- Zhai, E., Davis, C. A., Yan, L., and Hu, J. (2014). "Numerical simulations of geotechnical centrifuge modeling of seismic earth pressures on an underground restrained structure." *Int. Efforts in Lifeline Earthquake Engineering*, ASCE, Reston, VA, 369–376.